J Mol Model (2012) 18:4591–4601
DOI 10.1007/s00894-012-1453-9

ORIGINAL PAPER

Some insights into the binding mechanism of Aurora B kinase gained by molecular dynamics simulation

Rui Xiong · Xiao-Mei Cai · Jing Wei · Peng-Yu Ren

Received: 9 March 2011 / Accepted: 30 April 2012 / Published online: 30 May 2012

Abstract Aurora B kinase is essential in the process of mitosis, and its overexpression has been reported to be associated with a number of solid tumors. We therefore carried out molecular docking, molecular dynamics, and molecular mechanics Poisson–Boltzmann/surface area (MM-PBSA) calculations on several structurally diverse inhibitors (pentacyclic, pyrimidine, quinazoline, and pyrrolopyridine derivatives) and Aurora B kinase to explore the structural and chemical features responsible for the binding recognition mechanism. Molecular simulations reveal that the binding site mainly consists of six binding regions (sites A–F). We have identified that sites B and C are required for optimum binding in Aurora B–inhibitor complexes, sites A and F are needed to improve pharmacokinetic properties, while sites D and E lead to enhanced stability. We verified that hydrogen bonding to the hinge region and hydrophobic contact with the conserved hydrophobic pocket are of critical importance in the systems studied. Specifically, the amino acids Glu171, Phe172, and Ala173 in the hinge region and Leu99, Val107, and Leu223 in the conserved hydrophobic pocket probably account for the high binding affinities of these systems, as shown by hydrogen-bonding analysis and energy decomposition analysis. Hydrophobic contact with Phe172 is also in agreement with experimental data. In addition, the MM-PBSA calculations reveal that the binding of these inhibitors to Aurora B kinase is mainly driven by van der Waals/nonpolar interactions. The findings of this study should help to elucidate the binding pattern of Aurora B inhibitors and aid in the design of novel active ligands.

Keywords Aurora B kinase · Kinase inhibitor · Molecular docking · Molecular simulation · MM-PBSA · Energy decomposition

Electronic supplementary material The online version of this article (doi:10.1007/s00894-012-1453-9) contains supplementary material, which is available to authorized users.

R. Xiong · X.-M. Cai · J. Wei (✉)
Tianjin Key Laboratory for Modern Drug Delivery and High Efficiency, School of Pharmaceutical Science and Technology, Tianjin University,
Tianjin 300072, People's Republic of China
e-mail: tjucadd@yahoo.com.cn

P.-Y. Ren
Department of Biomedical Engineering, University of Texas, Austin, TX 78712, USA
e-mail: pren@mail.utexas.edu

Introduction

The Aurora kinases, a family of serine/threonine kinases, play a critical role in multiple aspects of mitosis in eukaryotic cells [1]. Humans express three Aurora kinases: Aurora A, B, and C, which exhibit 67–76 % amino acid sequence identity in their catalytic domains, but differ in amino acid length and sequence at the N-terminal domain [2]. Aurora A, the "polar kinase," localizes on centrosomes, and plays a crucial role in each step during mitosis. Aurora B, the "equatorial kinase," is a chromosomal passenger protein that moves from centromeres to the spindle midzone during mitosis. Although little is known about the importance of Aurora C, it is specifically expressed in the testis, and plays a role in spermatogenesis [3].

Deregulation of Aurora kinases due to genetic amplification and protein overexpression results in aneuploidy, and may contribute to tumorigenesis. A large amount of evidence indicates that Aurora kinases are overexpressed in a variety of solid tumors, including colon, breast, pancreas, prostate, pancreas, and thyroid cancers [1, 4]. As a result,

Aurora kinases have attracted considerable attention as potential targets for cancer chemotherapy.

In recent years, a number of small-molecule inhibitors targeting Aurora kinases have been developed, which can be subdivided into three general classes [5]: selective Aurora A inhibitors such as MLN8054 [6], selective Aurora B inhibitors such as hesperadin [7] and AZD1152 [8], and dual Aurora A/B inhibitors such as VX-680 [9] and ZM447439 [10]. The great majority of these synthetic Aurora kinase inhibitors are ATP-competitive, and have a planar heterocyclic ring system that is able to occupy the adenino-binding region and mimic adenine–kinase interactions. These inhibitors can be grouped according to the nature of their central heterocyclic moiety: indole derivatives, bis-indole derivatives, pyrimidine derivatives, pyrrolopyrazole derivatives, quinazoline derivatives, thiazoloquinazoline derivatives, pyrazoloquinazoline derivatives, fused tricyclic derivatives, and some other structures [11].

A thorough understanding of ligand-binding sites may aid the rational design of novel antitumor drugs and accelerate important therapeutic breakthroughs. In the last decade, the interaction between Aurora kinases and their inhibitors have been explored by X-ray crystallography and molecular modeling studies [12–16], especially for Aurora A kinase. Ligand-binding sites can be divided into two broad classes according to the conformation of the activation loop and region of the ATP site occupied by the inhibitor: those that bind at the ATP-binding site and those that bind at the activation loop [17].

However, only a few X-ray crystal structures of inhibitors complexed with Aurora B have been reported up to now. Previous studies have covered different chemical classes of inhibitors, such as indoles (hesperadin, PDB ID: 2BFY [14]), quinazolines (ZM447439, PDB ID: 2VRX [13]), and purine derivatives (PDB ID: 2VGO [18]). The binding modes of Aurora B with other kinds of inhibitors remain unknown. To obtain new insights into these inhibitor–Aurora B kinase interactions, we have carried out a theoretical study employing molecular docking and molecular dynamics approaches. The study aimed to elucidate the binding mechanism of inhibitors toward Aurora B kinase based on their molecular dynamics, and the results from this study are reported below.

Materials and methods

Structure preparation

The X-ray crystal structure of Aurora B kinase in complex with ZM447439 (**1**, PDB ID: 2VRX) was obtained from the RCSB Protein Data Bank. Aurora B inhibitor ZM447439 was removed from the complex structure in order to model the protein structure in this study.

We collected a series of structurally diverse Aurora B inhibitors (**2**–**5**) with representative biological activities [5, 19, 20], including pentacyclic derivatives, pyrimidine derivatives, quinazoline derivatives, and pyrrolopyridine derivatives. Their chemical structures are listed in Fig. 1. All of the Aurora B kinase inhibitors were built using a 2D/3D editor sketcher and energy minimized to a local energy minimum using the CHARMm-like force field implemented within the Catalyst 4.11 software package.

Automated flexible-ligand docking

To explore the probable active site of the Aurora B kinase, flexible-ligand docking was initially performed in the AutoDock 4.0 software package, and then energy-optimized ligands were docked into the potential binding sites of Aurora B kinase.

Polar hydrogen atoms were added, nonpolar hydrogen atoms were merged, and Gasteiger charges were assigned by default. All docking calculations were performed with the Lamarckian genetic algorithm (LGA) [21]. A population size of 300 and 25,000,000 energy evaluations were used for 100 search runs. The grid dimensions were 50 × 50 × 50 points along the *x*-, *y*-, and *z*-axes, and a grid spacing of 0.375 Å was used. The conformations with the lowest docked energies and reasonable orientations in light of the nature of the ATP-binding pocket were chosen for subsequent analysis.

Molecular dynamics (MD)

Based on the docking results, four Aurora B–inhibitor systems (Aurora B complexed to compounds **2**–**5**) were subjected to molecular dynamics simulations using the SANDER module of the Amber 10 package. The amber99SB force field was used for the protein and the general AMBER force field (GAFF) [22] for the inhibitors. All of the complexes were solvated in TIP3PBOX water [23], ensuring that the box surfaces were at least 10 Å away from any protein and ligand atoms. Counterions (Na^+) were added to neutralize the charge of the system. All covalent bonds containing the hydrogen atoms were constrained using the SHAKE algorithm [24]. The particle mesh Ewald method [25] was used to treat the long-range electrostatic interaction, with a cutoff distance of 8 Å. Energy minimization was achieved in three steps. First, movement was only allowed for the water molecules and ions. Next, the ligand and the receptor residues were allowed to move in addition to the water molecules and ions. Finally, all atoms were permitted to move freely. Energy minimization was performed to release the bad contacts in the crystallographic structure, and the convergence criterion for the energy gradient was 1.0×10^{-4} cal mol^{-1} A^{-1}. Subsequently, the

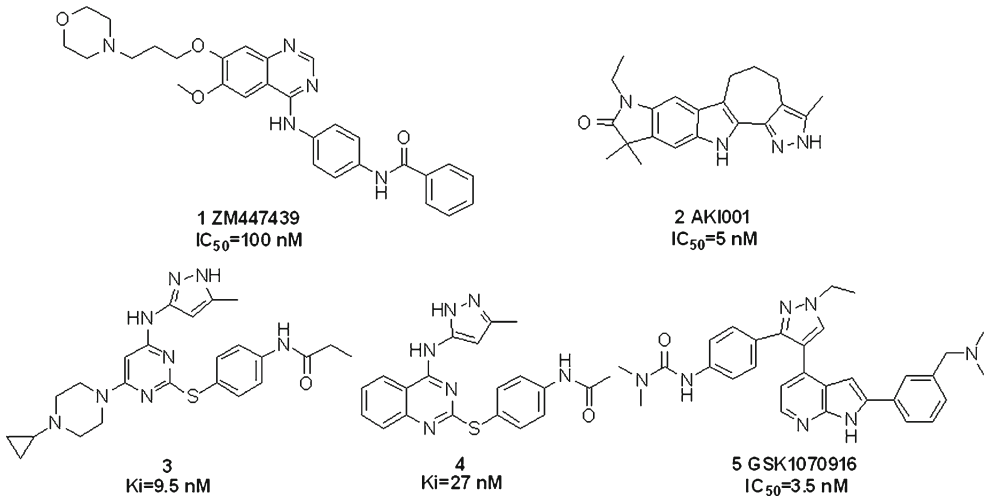

Fig. 1 Structures of the Aurora B kinase inhibitors studied in this work

complexes of the minimized structure were subjected to 3000 ps MD simulations at 300 K and a pressure of 1 bar. An integration step of 2 fs was used.

Free-energy analysis by the MM-PBSA method

The free-energy calculations of inhibitors binding to Aurora B kinase were performed by the molecular mechanics Poisson–Boltzmann surface area (MM-PBSA) method in Amber 10 [26, 27]. The binding free energy was calculated as the average binding free energy of the last 2 ns, collected at 2 ps intervals during the trajectories. The full thermodynamic process is given below:

$$\begin{array}{ccc} Rec_{aqu} + Lig_{aqu} & \xrightarrow{\Delta G_{binding}} & Rec/Lig_{aqu} \\ \downarrow -\Delta G_{sol}^{\mathrm{Rec}} & \downarrow -\Delta G_{sol}^{Lig} & \downarrow -\Delta G_{sol}^{\mathrm{Rec}/Lig} \\ Rec_{gas} + Lig_{gas} & \xrightarrow{\Delta Ggas} & Rec/Lig_{gas}. \end{array}$$

The total free energy of binding consisted of the following terms:

$$\Delta G_{\mathrm{b}} = \Delta E_{\mathrm{MM}} + \Delta G_{\mathrm{sol}} - T\Delta S \tag{1}$$

$$\Delta E_{\mathrm{MM}} = \Delta E_{\mathrm{int}}^{\mathrm{ele}} + \Delta E_{\mathrm{int}}^{\mathrm{vdw}} \tag{2}$$

$$\Delta G_{\mathrm{sol}} = \Delta E_{\mathrm{sol}}^{\mathrm{ele}} + \Delta E_{\mathrm{sol}}^{\mathrm{nonpol}} \tag{3}$$

$$\Delta E_{\mathrm{sol}}^{\mathrm{nonpol}} = \gamma A + b, \tag{4}$$

where ΔG_{b} is the binding free energy in solution; ΔE_{MM} is the molecular mechanical energy, comprising the electrostatic and van der Waals interaction energies $\left(\Delta E_{\mathrm{int}}^{\mathrm{ele}} + \Delta E_{\mathrm{int}}^{\mathrm{vdw}}\right)$ between the ligand and the protein; and ΔG_{sol} is the solvation energy, which contains the electrostatic contribution and the hydrophobic contribution to the solvation free energy $\left(\Delta G_{\mathrm{sol}}^{\mathrm{ele}} + \Delta G_{\mathrm{sol}}^{\mathrm{nonpol}}\right)$. The electrostatic solvation energy is determined using the finite difference Poisson–Boltzmann (PB) or generalized Born (GB) method, and the nonpolar contribution is estimated by the solvent-accessible surface area (SASA) method. In this work, the energy contribution from entropy changes upon the binding of the ligand was not included. This was justified by the fact that it is likely that the entropy makes only a minor contribution to the relative binding free energies of the ligands to the same protein, and the good agreement between the calculated and experimental relative binding energies obtained upon applying the same approximation in several earlier studies [28]. The calculated error bars are standard errors of the mean (SE):

$$SE = \frac{\text{standard deviation(STD)}}{\sqrt{N}}, \tag{5}$$

where N is the number of trajectory snapshots used in the calculations.

Inhibitor–residue interaction decomposition

The interactions between the inhibitors and each residue in Aurora B kinase were analyzed using the MM-GBSA module in Amber 10. The energy decomposition calculation analyzed the same snapshots as those used in the free-energy calculation [29, 30]. The binding interaction of each inhibitor–residue pair includes four terms:

$$\Delta G_{\mathrm{inhibitor-residue}} = \Delta G_{\mathrm{vdw}} + \Delta G_{\mathrm{ele}} + \Delta G_{\mathrm{pol}} + \Delta G_{\mathrm{nonpol}}. \tag{6}$$

where the van der Waals contribution (ΔG_{vdw}) and the electrostatic contribution (ΔG_{ele}) can be calculated using the Sander program in Amber 10.0. The polar solvation contribution (ΔG_{pol}) was computed using the generalized Born module. The nonpolar solvation contribution ($\Delta G_{\mathrm{nonpol}}$) is the nonpolar contribution to the solvation free energy.

Results and discussion

Stability of the Aurora B–inhibitor complexes

Molecular docking calculations were first performed for a series of inhibitors (compounds **2**–**5**) without explicit active-site water molecules. The ligand structures with the most favorable binding free energies and reasonable orientations were selected as the optimal docked conformations. To acquire the binding mode of the ligand–Aurora B kinase complex, we took the flexibility of the protein into consideration, and selected the optimal docked conformations of four representative compounds (compounds **2**–**5**) on which to perform MD simulation.

3 ns MD simulations were successfully performed on four Aurora B–inhibitor complexes. To gauge whether the MD simulations were stable and whether they converged, energetic and structural properties were monitored during the course of MD simulation. The small root-mean-square deviation (RMSD) fluctuations and the convergence in the energies, temperatures, and pressures of the systems observed indicate well-behaved systems. The RMSDs between the Cα, C, and N atoms of the structures obtained during the trajectories and the initial structures are shown in Fig. 2 for the four systems. The averaged RMSD during the last 2 ns for Aurora B/compound **2**, Aurora B/compound **3**,Aurora B/compound **4** and Aurora B/compound **5** complexes are 1.54, 1.60, 1.56 and 1.36 Å, respectively, suggesting the overall stable structures after approximately 2 ns simulation, which is also validated by the unchanged distances of four compounds with key residues measured in hydrogen analysis part.

Architecture of the Aurora B kinase binding site

During the analysis, the molecular superposition of bound conformations of compounds from different classes (Fig. 3) indicated that these inhibitors have different binding orientations in the binding pocket of Aurora B kinase. The active site of Aurora B kinase lies at the interface between the N-terminal lobe (residues 86–174) and the C-terminal lobe (residues 175–347), which is similar to the ATP-binding pocket. The N-terminal lobe is implicated in nucleotide binding, and interacts with kinase regulators. The C-terminal lobe serves as a docking site for substrates, and contains residues that direct phosphate transfer [14]. Figure 3 shows that the amino acids of the binding site in the four complexes overlap to a large extent, but that the side chain of Lys122 in the Aurora B–compound **2** complex shifts noticeably to the left.

Figure 4 illustrates the six main sites A–F on the surface binding groove of Aurora B kinase. Site A is the solvent-exposed front pocket created by residues Arg97, Leu99, Gly100, Arg175, Gly176, and Glu177, which is reported to be a major contributor to the enhanced affinity of a series of 7-substitued indirubins [31]. Site B is mainly associated with the H-bonding network in the hinge region (formed by 171–174), where the inhibitors bind to the active site of Aurora B kinase by forming direct hydrogen bonds with the main chain amides of Glu171 and Ala173, which are also observed in the binding mode of the ATP–Aurora A complex (Glu211 and Ala213 in Aurora A kinase) [12, 32]. This part of the hinge region is structurally conserved in many other kinases too, such as SRC kinase, cyclin-dependent kinase 2, and glycogen synthase kinase-3β [33]. Site C is referred to as a conserved hydrophobic back pocket, as formed by Leu99, Val107, Ala120, Leu154, Leu170, and Leu223. Site D is a selective binding pocket formed by Leu223, Ala233, and Asp234. Site E is another selective hydrophobic pocket formed by the residues Leu138, Ile142, and Leu168. Site F is a highly solvent-exposed phosphate binding region that is mainly formed by Lys122 and Glu141, and is larger than the solvent-exposed front pocket. Our proposals for the binding mode are basically in accord with the ATP-binding pocket reported by Garuti's group [11], which consists of subsites including the adenine pocket (corresponding to site B), the ribose region (corresponding to site C), the buried groove region (corresponding to site F), and the solvent-accessible region (corresponding to site A).

Essentially, sites A, B, and F tend to form hydrogen bonds, while the other sites stabilize the kinase–inhibitor complex through hydrophobic interactions. It is expected that the selective hydrophobic pocket sites D and E can be exploited to enhance the stability of the Aurora B–inhibitor complex, while the highly solvent-exposed sites A and F may improve the pharmacokinetic properties of the lead compounds.

Binding mode analysis

Binding mode of the pentacyclic inhibitor (compound 2)

Figure 3 shows the model of the pentacyclic inhibitor (compound **2**) binding at the active site of Aurora B kinase. Compound **2** binds in a deep, catalytic active site formed by the hinge region through five hydrogen bonds (shown in Fig. 5a). The oxygen atom of carbonyl group forms two hydrogen bonds with Arg97 (NH1) and Arg97 (NH2) in the solvent-exposed front pocket. The amino function of the pyrrole ring forms a hydrogen bond with the backbone Ala173. The N atoms of the pyrazole ring are hydrogen bonded to the backbone of Ala173 and Glu171, respectively. The tail segment faces toward the solvent-accessible region (site A) and is surrounded by Arg97, Leu99, Arg175, and Gly176. The phenyl ring

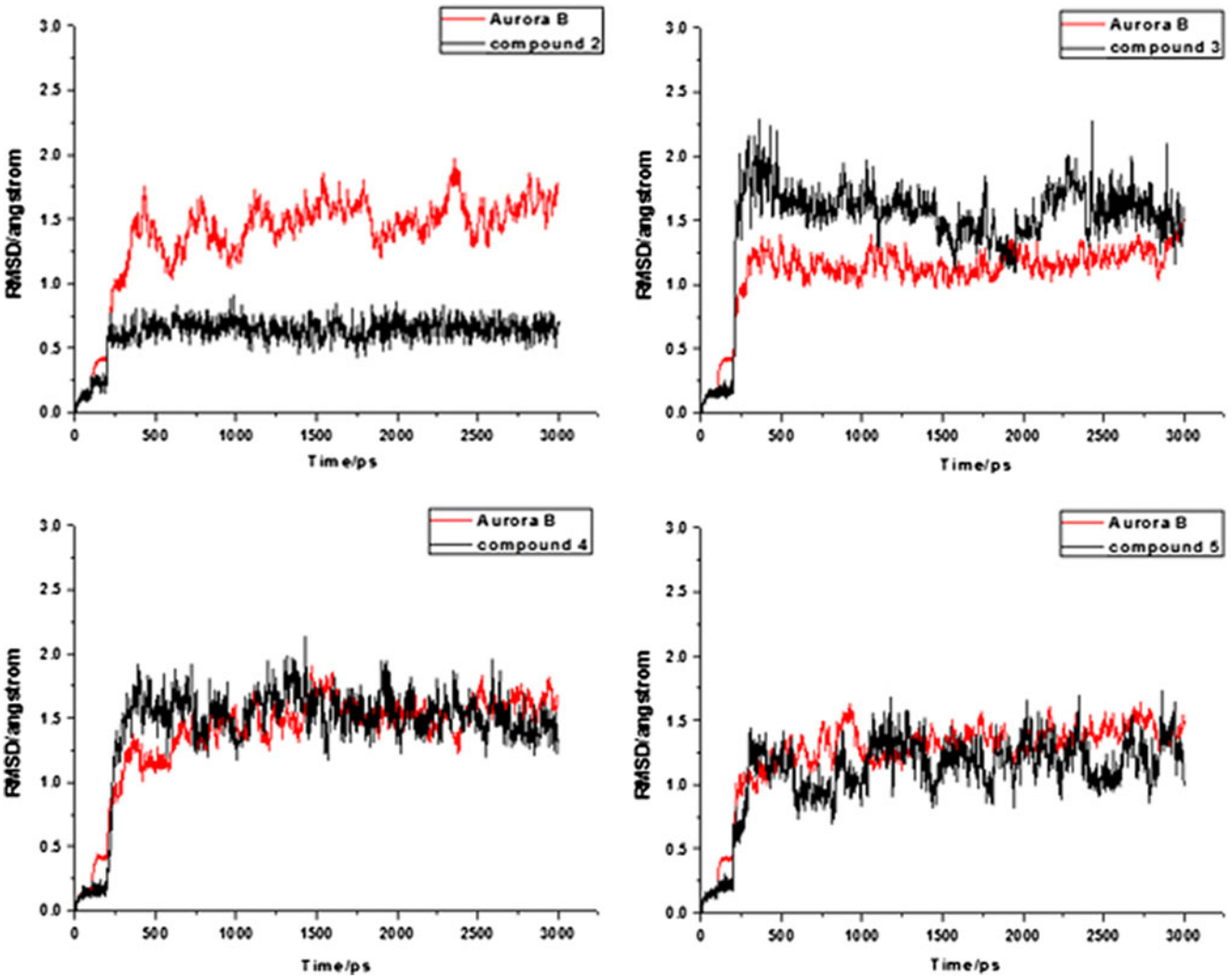

Fig. 2 Time dependences of the root-mean-square deviations (RMSDs) of the Cα, C, and N atoms of the four systems from the starting structure

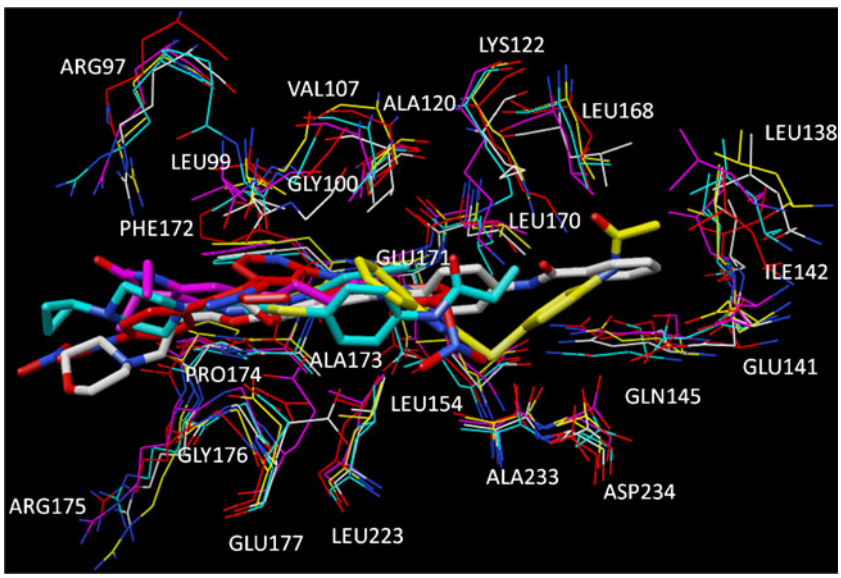

Fig. 3 Superposition of binding conformations of inhibitors extracted from the last snapshot taken during the MD simulation. Active-site amino acid residues are represented as *wires* and inhibitors are shown as *sticks*. The complexes are color-coded as follows: *white* compound **1**, *magenta* compound **2**, *cyan* compound **3**, *yellow* compound **4**, *red* compound **5**

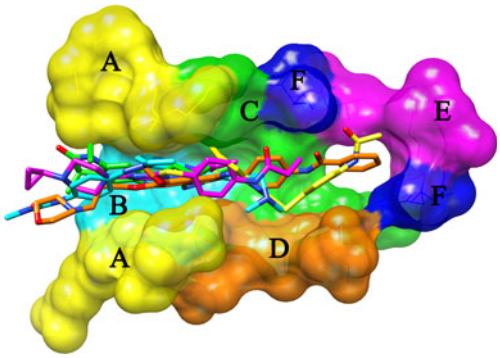

Fig. 4 The six active binding regions, color-coded as follows: *yellow* site A, *cyan* site B, *green* site C, *orange* site D, *magenta* site E, *blue* site F

moiety of compound **2** is sandwiched by the side chains of Leu99, Phe172, and Gly176. The cycloheptane ring undergoes favorable hydrophobic interactions with Leu99, Val107, and Leu223. The binding is stabilized by the hydrophobic contact of the pyrazole segment with Lys122, Leu154, and Leu170.

The crystal structure of the Aurora A–compound **2** complex has already been solved and was gained from the Protein Data Bank (PDB code 3COH). To throw light on the differences between two Aurora kinases, we performed a comparative study of the structures of the Aurora A–compound **2** and Aurora B–compound **2** complexes. The binding domain shows a slight difference in sequence identity between these two Aurora kinases. One amino acid differs in the binding domain: it is Y212 in Aurora A and F172 in Aurora B. A shift in the positions of residues is observed in the binding domain of Aurora A when compared with that of Aurora B (Fig. S1 of the "Electronic supplementary material," ESM). Nonetheless, superimposing the two complex structures illustrates that compound **2** maintains a similar binding mode in the two Aurora kinases. Similar hydrogen bonds between compound **2** and Glu211/Ala213 are seen for Aurora A. The hydrophobic interactions are conserved for the two Aurora kinases. These observations are in agreement with Cochran's research [19]. Interestingly, the side chain of Arg137 in Aurora A adopts a different relative orientation (it is rotated by about 90°), resulting in a lack of H-bonding between Arg137 and compound **2**, in contrast with Aurora B (Fig. S1 of the ESM). This difference may facilitate the design of an Aurora subtype-selective antitumor drug.

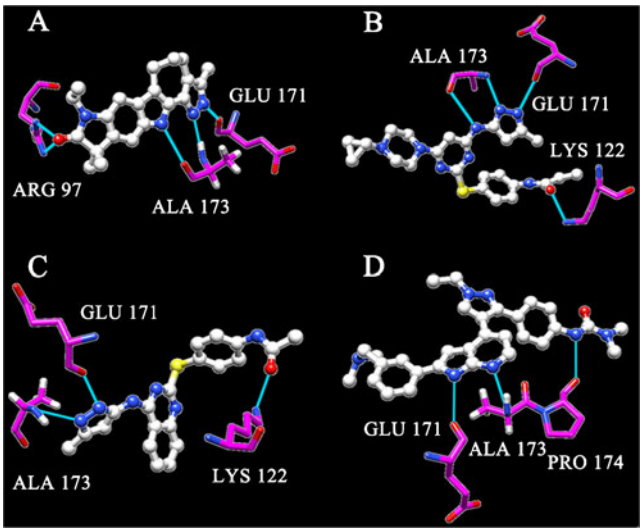

Fig. 5 The hydrogen-bonding interactions (*cyan lines*) between the inhibitors and Aurora B kinase. **a** compound **2**, **c** compound **3**, **c** compound **4**, **d** compound **5**

Binding mode of the 2,4,6-trisubstituted pyrimidine inhibitor (compound 3)

The model of compound **3** bound to Aurora B kinase at the active site is shown Figs. 3 and 5b. The NH and N of the pyrazole group are hydrogen bonded to the backbone O atom of Glu171 and the backbone NH of Ala173. The NH group linking the pyrimidine ring and the pyrazole ring forms a hydrogen bond with the backbone O of Ala173. The oxygen atom of the carbonyl group forms a hydrogen bond with Lys122NZ. The pyrazole moiety undergoes a hydrophobic interaction with the lipophilic cage made up of Val107, Ala120, Leu170, Phe172, and Leu223. The phenyl ring participates in favorable hydrophobic interactions with Val107 and Leu223. The piperazine ring is positioned in the solvent-exposed front pocket and is surrounded by Arg97, Leu99, and Gly176. The cyclopropyl ring protrudes out toward the solvent, similar to the solubilizing morpholine of compound **1**.

Binding mode of the 2-phenylthioquinazoline inhibitor (compound 4)

Figures 3 and 5c show a close-up view of the binding interaction of Aurora B kinase with compound **4**. The pyrazole ring undergoes hydrophobic interactions with the side chains of the residues Leu154, Phe172, Ala173, and Leu223. The NH and N in the pyrazole ring are stabilized by hydrogen-bonding interactions with the main chains of Glu171 and Ala173, respectively. The phenyl ring of the central quinazoline group is anchored by hydrophobic interactions with Gly100, Val107, and Leu223. The benzenethiol group binds the neighboring residues Ala233 and Asp234. The acetamide moiety of compound **4** extends into the active site E, formed by Leu138, Ile142, and Leu168. The oxygen atom of the carbonyl group forms a hydrogen bond with the side chain of Lys122 (NZ).

Binding mode of the pyrrolopyridine derivative inhibitor (compound 5)

Figure 3 illustrates the binding mode of compound **5** with the active site of Aurora B kinase. The central 1*H*-pyrrolo[2,3-*b*] pyridine ring is located in the vicinity of the hinge region and forms two hydrogen bonds with the backbones of Glu171 and Ala173 (Fig. 5d), respectively. The pyridine ring also shows a T-shaped π–π stacking interaction with Phe172. The 1,1-dimethyl-3-phenylurea moiety is positioned in the solvent-exposed front pocket, and makes contact with Arg175 and Gly176. Also, the NH group of the moiety forms a hydrogen bond with the backbone of Pro174. Our result is in good agreement with the structure–activity relationship reported by WeiMin Chen et al., which revealed that hydrogen-bond-based binding regions at the 1*H*-pyrrolo[2,3-*b*]pyridine ring and the urea group increase activity [34]. However, their docking results suggested that the ethylcarbamylamino group formed three H-bonds with Ala223, Gln145, and Lys122. The 1-ethyl-1*H*-pyrazole moiety is sandwiched by the side chains of Leu99, Gly100, and Glu177. The phenyl ring of the *N*,*N*-dimethyl-1-phenylmethanamine moiety undergoes a hydrophobic interaction with the hydrophobic pocket created by Val107, Leu154, Leu170, and Leu223, and the substituent of the phenylmethanamine moiety faces toward site D, consisting of Ala233 and Asp234.

Hydrogen bonds between Aurora B and inhibitors

Hydrogen bonds play an essential role in stabilizing protein–ligand complexes. We investigated the geometry and stability of the hydrogen-bond network formed by the inhibitor in the ATP-binding pocket. The hydrogen bonds (shown in Fig. 5) were examined on the basis of the trajectories of the MD simulations (1000 snapshots). In Table 1, the Aurora B–inhibitor H-bond contacts are characterized in terms of the distances between heavy atoms and their percentages of occurrence. To identify hydrogen bonds, a distance cutoff of about 2.5 Å and an angle (D–H–A) of >120° were used.

For compound **2**, two significant hydrogen bonds are formed through the pyrazole ring N and the pyrrole ring NH to Ala173NH (97.8 % bond occupancyduring the MD simulation) and Ala173O (94.0 % occupancy), respectively. For compound **3**, two hydrogen bonds with Ala173 are preserved, with occurrence frequencies of 99.0 % and 95.5 %, respectively. Compounds **4** and **5** are both hydrogen bonded to the main chain of Ala173 (96.2 % and 99.0 % occupancy, respectively). These results suggest that the hydrogen bond with Ala173 is sturdy and can stabilize the binding of the ligands to Aurora B kinase. In addition, compounds **2**–**5** form hydrogen bonds with Glu171, which are present in 99.8 %, 98.6 %, 92.1 %, and 24.4 % of the computed snapshots during the MD simulation, respectively. In compound **5**, the hydrogen bond with Glu171 is weaker than those with other inhibitors, but the hydrogen bond with Pro 174 (61.9 % occupancy) enhances the stability of the H-bonding network in the hinge region.

Two hydrogen bonds between the carboxyl group of compound **2** and the NH groups of Arg97 (CO…NH1 Arg97 and CO…NH2 Arg97) are present in only 5.7 % and 7.4 % of the computed snapshots, respectively. Their percentages of occurrence suggest that these two hydrogen bonds can be considered transient due to the high flexibility of Arg97 in the solvent-exposed front pocket. Additionally, the hydrogen bond between compound **3**/**4** and Lys122 was found to be transient, with an occurrence frequency of only

Table 1 Hydrogen bond analysis

Inhibitor	Donor[a]	Acceptor H	Acceptor	Distance (Å) (% occupied[b])	Angle (°)
Compound **2**	171Glu:O	Com2:H22	Com2:N1	2.90(99.8)	17.08
	Com2:N2	173Ala:H	17:N	3.05(97.8)	24.61
	173Ala:O	Com2:H23	Com2:N3	2.97(94.0)	39.76
	Com2:O	97Arg:HH22	97Arg:NH2	3.12(7.40)	43.73
	Com2:O	97Arg:HH12	97Arg:NH1	3.13(5.70)	46.12
Compound **3**	Com3:N4	173Ala:H	173Ala:N	2.93(99.0)	25.77
	171Glu:O	Com3:H6	Com3:N3	3.00(98.6)	22.47
	173Ala:O	Com3:H4	Com3:N2	3.09(95.5)	21.92
	Com3:O	122Lys:HZ2	122Lys:NZ	2.94(12.6)	33.71
Compound **4**	Com4:N4	173Ala:H	173Ala:N	3.09(96.2)	28.30
	171Glu:O	Com4:H12	Com4:N5	3.06(92.1)	31.04
	Com4:O	122Lys:HZ1	122Lys:NZ	2.85(23.0)	25.61
Compound **5**	Com5:N2	173Ala:H	173Ala:N	3.05(99.0)	16.42
	174Pro:O	Com5:H27	Com5:N5	3.09(61.9)	34.27
	171Glu:O	Com5:H11	Com5:N3	3.30(24.4)	19.44

[a]The combination of a donor atom D, a hydrogen atom H, and an acceptor atom A in a D–H…A configuration was regarded as a hydrogen bond when the distance between the donor D and the acceptor A was shorter than R_{max} (=3.5 Å) and the angle H–D–A was smaller than θ_{max}(=60.0°). Symbols for the residues are explained in the text

[b]The percentage of the MD simulation during which the hydrogen bond existed, which was used to evaluate the stability and the strength of the hydrogen bond during the MD simulation

12.6/23.0 %, which may also reflect the flexibility of the Lys122 in the highly solvent-exposed phosphate-binding region.

In conclusion, Glu171 and Ala173 are observed to be firmly and solidly hydrogen bonded to ligands, and they are also observed in the complexes of the inhibitors with Aurora A (corresponding to Glu211 and Ala213) [11, 13, 19]. However, the hydrogen bonds between ligands and Lys122/Arg97 located within the solvent-accessible region were found to be transient or moderate, reflecting the high conformational flexibility of the amino acids near the surface compared to those buried in the hinge region.

MM/PBSA free-energy analysis

Further insights into the forces involved in substrate binding can be obtained by analyzing the MM/PBSA free-energy contributions. Table 2 lists the individual energy components of the calculated binding free energies for the four inhibitor complexes. For compounds **2**–**5**, the calculated binding free energies (ΔG_b) of their complexes with Aurora B kinase are −36.42, −28.43, −27.20, and −27.66 kcal mol^{-1}, respectively. Considering the fact that there are minor differences between the activity data provided by different scientific groups (as shown in Fig. 1), we did not analyze the relationship between the calculated binding free energies and experimental biological activities.

In all four kinase–inhibitor complexes, the intermolecular van der Waals interactions (ΔE_{int}^{vdw}) make the most significant contribution by far to the binding free energies, whereas the overall electrostatic interaction energies (ΔG_{ele}) are positive and unfavorable for the binding free energies (showed in Table 2). Nonpolar solvation terms, which correspond to the burial of SASA upon binding, contribute slightly favorably. However, the total affinity arises from a more complex interplay between all of these components.

Free-energy decomposition analysis

To characterize the different contributions to the binding free energies of compounds **2**–**5** with Aurora B kinase, absolute binding free energies were calculated for the four complexes by the MM/GBSA method. The binding free energy was decomposed into inhibitor–residue pairs in order to generate an inhibitor–residue interaction spectrum. Figure 6 shows the decomposition of ΔG_b values on a per residue basis for residues with $|\Delta G_b|$ >1.0 kcal mol^{-1} in the four complexes. Tables S1–4 illustrate the energy contributions of certain structurally important residues for the Aurora B–inhibitor interactions. The decomposition approach was helpful for locating residues that contribute to the Aurora B–inhibitor interaction.

For compounds **2**–**5**, the major binding attractions come from the residues Glu171, Phe172, and Ala173 of site B and Leu99, Val107, and Leu223 of site C, suggesting that they play an important role in the binding. For Glu171 and Ala173, the favorable forces are electrostatic energies. This phenomenon can be explained by the fact that Ala173 is observed to hydrogen bonded to four systems and Glu171 is observed to hydrogen bond to three systems. Phe172 and Leu223 are the important amino acids that make the greatest contributions to the binding affinities. The importance of Phe172 is also supported by the results of a single-mutation experiment in Girdler's work, which indicate that F172H mutation can weaken biological activity by reducing the van der Waals interactions with the inhibitors and steric hindrance [13]. The main force for amino acid Leu223 is the van der Waals energy. In addition, the van der Waals energies are the dominant forces that drive the binding of the inhibitors (specifically compounds **2**, **3**, and **5**) to Leu99 and Val107. The above results obviously indicate that site C is the most important binding region for hydrophobic recognition among the six sites.

Gly176 plays an important role in site A, except with compound **4**, which hardly interacts with active site A. The

Table 2 Individual energy components for the calculated binding free energies ΔG (kcal mol^{-1})

Contribution	Compound **2**	Compound **3**	Compound **4**	Compound **5**
ΔE_{int}^{ele}	−25.48(0.13)	81.50(0.40)	−44.52(0.20)	27.44(0.55)
ΔE_{int}^{vdw}	−41.61(0.08)	−42.53(0.09)	−42.99(0.10)	−46.31(0.10)
ΔG_{sol}^{nonpol}	−5.51(0.01)	−6.35(0.01)	−6.58(0.01)	−7.25(0.01)
ΔG_{sol}^{ele}	36.17(0.13)	−61.05(0.37)	66.89(0.21)	−1.55 (0.79)
ΔG_{sol} [a]	30.67(0.13)	−67.40(0.37)	60.31(0.21)	−8.79(0.78)
ΔG_{ele} [b]	10.70(0.10)	20.45(0.13)	22.37(0.15)	25.89(0.53)
ΔG_b	−36.42(0.11)	−28.43(0.12)	−27.20(0.14)	−27.66(0.53)

[a] The polar/nonpolar $\left(\Delta G_{sol}^{ele} + \Delta G_{sol}^{nonpol}\right)$ contributions

[b] The electrostatic $\left(\Delta E_{int}^{ele} + \Delta G_{sol}^{ele}\right)$ contributions. All energies are averaged over 1000 snapshots and are given in kcal mol^{-1}.

ΔG_b does not explicitly consider entropy contributions. The values in parentheses represent the standard error of the mean

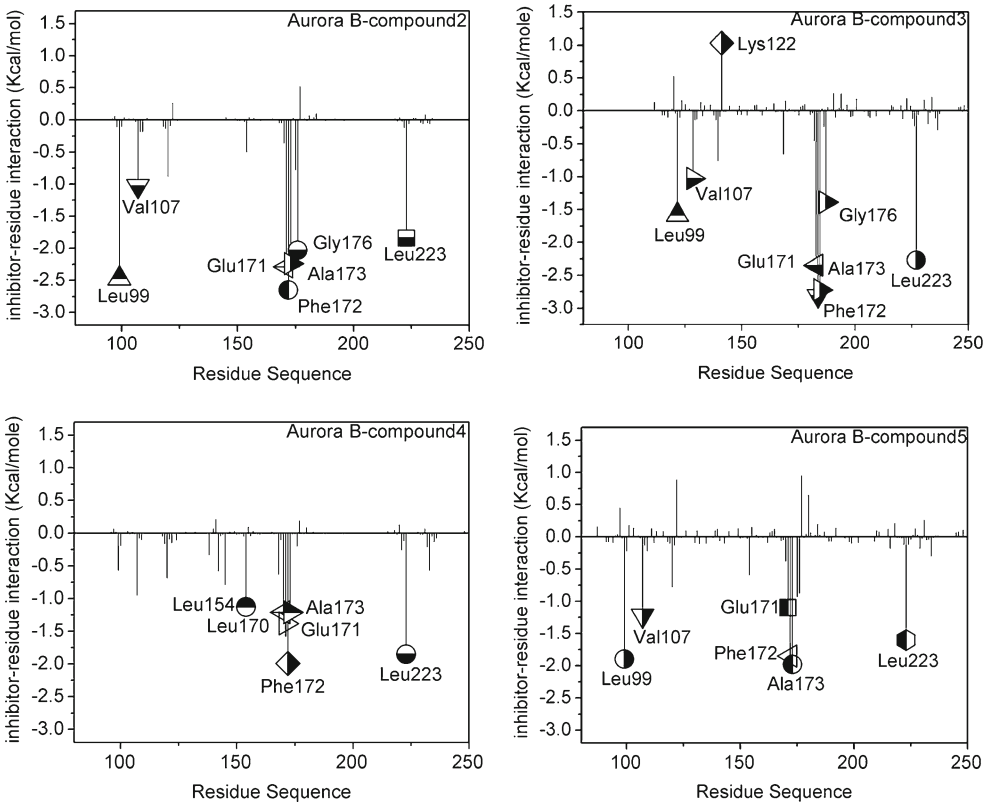

Fig. 6 Decomposition of $\Delta G_{\text{inhibitor–residue}}$ on a per residue basis for complexes of Aurora B with compounds **2**, **3**, **4**, and **5**

main determinant for amino acid Gly176 is the van der Waals energy, for which decomposed ΔG_b values are −1.45 kcal mol^{-1} for compound **2**, −1.50 kcal mol^{-1} for compound **3**, and −0.87 kcal mol^{-1} for compound **5**, respectively. For the Aurora B–compound **4** system, Leu154 and Leu170 are the most important amino acids for the binding affinity. The decomposed ΔG_b value for Lys122 varies widely, mainly due to its flexibility.

As shown in Fig. 6, the residues with the most favorable contributions in all four Aurora B–inhibitor systems are Leu99, Val107, Glu171, Phe172, Ala173, and Leu223. Based on the binding modes, a protein-based pharmacophore model hypothesis was derived. This hypothesis consists of six slightly different pharmacophore hypotheses (shown in Fig. 7): one hydrogen-bond acceptor feature (corresponding to Ala173NH), two hydrogen-bond donor features (corresponding to Ala173O and Glu171O), and three hydrophobic features (corresponding to the hydrophobic regions formed by Val107, Phe172/Leu223, and Leu99/Phe172/Gly176, respectively).

Based on our studies, we were able to suggest fragments that should increase the binding affinity at sites D, E, and F. For example, we designed a new compound with an *N*-(4-mercaptophenyl)acetamide substituent at the cycloheptane ring of compound **2**. This compound showed a greatly enhanced binding energy, and the *N*-(4-mercaptophenyl) acetamide substituent was located in sites E and F and anchored by hydrogen bonds with Lys122NZ and Asp234OD2 (see Fig. S1 in the ESM).

Conclusions

We have performed molecular docking, molecular dynamics simulation, and MM-PBSA calculations, and developed binding modes for various types of Aurora B kinase inhibitors (pentacyclic, pyrimidine, quinazoline, and pyrrolopyridine inhibitors). Molecular binding-mode analysis indicated the

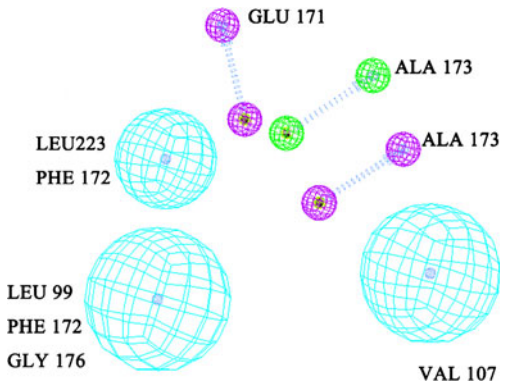

Fig. 7 Pharmacophore model. The features of the pharmacophore are color-coded: *green* represents a hydrogen-bond acceptor; *magenta* represents a hydrogen-bond donor; *light blue* represents a hydrophobic feature

existence of six binding sites (A: solvent-exposed front pocket, B: hinge region, C: conserved hydrophobic pocket, D and E: selective hydrophobic pockets, F: solvent-exposed phosphate-binding region). Among all of these sites, site C was observed to be the critical region for binding recognition, as it showed favorable hydrophobic interactions with all inhibitors. Hydrogen bonding to the hinge region was found to be more stable than that to the solvent-accessible region through hydrogen-bond analysis. Subsequent analysis of the separate energy terms contributing to the MM-PBSA free energy suggested that the association between Aurora B kinase and each inhibitor is mainly driven by favorable van der Waals and nonpolar interactions, whereas the electrostatic term opposes the binding. Specifically, the amino acids Leu99, Val107, Glu171, Phe172, Ala173, and Leu223 were found to be responsible for the high affinity of the interaction, as observed when dividing the binding free energy into individual components.

The inhibitors were all bound in the conserved hydrophobic pocket (site C), anchored by hydrophobic interactions with Leu99, Val107, and Leu223, and were stabilized by hydrogen-bonding interactions with the Glu171 and Ala173. We suggest that sites B and C are required for the optimum binding of novel Aurora B kinase inhibitors, sites A and F play important roles in improving the pharmacokinetic properties of lead compounds, while sites D and E appear to be selective hydrophobic pockets that enhance the stability of the Aurora B–inhibitor complexes.

Acknowledgments We gratefully acknowledge the support from the Project of Undergraduate Educational Reform and Capacities in Tianjin University (no. 200904050). PR acknowledges support from the National Institute of General Medical Sciences (R01 GM079686-04).

References

1. Ikezoe T (2008) Aurora kinases as an anti-cancer target. Cancer Lett 262:1–9
2. Carmena M, Earnshaw WC (2003) The cellular geography of aurora kinases. Nat Rev Mol Cell Biol 4:842–854
3. Ruchaud S, Carmena M, Earnshaw WC (2007) Chromosomal passengers: conducting cell division. Nat Rev Mol Cell Biol 8:798–812
4. Vader G, Lens SMA (2008) The Aurora kinase family in cell division and cancer. BBA-Rev Cancer 1786:60–72
5. Pollard JR, Mortimore M (2009) Discovery and development of aurora kinase inhibitors as anticancer agents. J Med Chem 52:2629–2651
6. Manfredi MG, Ecsedy JA, Meetze KA, Balani SK, Burenkova O, Chen W, Galvin KM, Hoar KM, Huck JJ, LeRoy PJ, Ray ET, Sells TB, Stringer B, Stroud SG, Vos TJ, Weatherhead GS, Wysong DR, Zhang MK, Bolen JB, Claiborne CF (2007) Antitumor activity of MLN8054, an orally active small-molecule inhibitor of aurora A kinase. Proc Natl Acad Sci USA 104:4106–4111
7. Hauf S, Cole RW, LaTerra S, Zimmer C, Schnapp G, Walter R, Heckel A, van Meel J, Rieder CL, Peters JM (2003) The small molecule Hesperadin reveals a role for aurora B in correcting kinetochore–microtubule attachment and in maintaining the spindle assembly checkpoint. J Cell Biol 161:281–294
8. Yang J, Ikezoe T, Nishioka C, Tasaka T, Taniguchi A, Kuwayama Y, Komatsu N, Bandobashi K, Togitani K, Koeffler HP, Taguchi H, Yokoyama A (2007) AZD1152, a novel and selective aurora B kinase inhibitor, induces growth arrest, apoptosis, and sensitization for tubulin depolymerizing agent or topoisomerase II inhibitor in human acute leukemia cells in vitro and in vivo. Blood 110:2034–2040
9. Harrington EA, Bebbington D, Moore J, Rasmussen RK, Ajose-Adeogun AQ, Nakayama T, Graham JA, Demur C, Hercend T, Diu-Hercend A, Su M, Golec JMC, Miller KM (2004) VX-680, a potent and selective small-molecule inhibitor of the Aurora kinases, suppresses tumor growth in vivo. Nat Med 10:262–267
10. Gadea BB, Ruderman JV (2005) Aurora kinase inhibitor ZM447439 blocks chromosome-induced spindle assembly, the completion of chromosome condensation, and the establishment of the spindle integrity checkpoint in *Xenopus* egg extracts. Mol Biol Cell 16:1305–1318
11. Garuti L, Roberti M, Bottegoni G (2009) Small molecule aurora kinases inhibitors. Curr Med Chem 16:1949–1963
12. Talele TT, McLaughlin ML (2008) Molecular docking/dynamics studies of aurora A kinase inhibitors. J Mol Graph Modell 26:1213–1222
13. Girdler F, Sessa F, Patercoli S, Villa F, Musacchio A, Taylor S (2008) Molecular basis of drug resistance in aurora kinases. Chem Biol 15:552–562
14. Sessa F, Mapelli M, Ciferri C, Tarricone C, Areces LB, Schneider TR, Stukenberg RT, Musacchio A (2005) Mechanism of aurora B activation by INCENP and inhibition by hesperadin. Mol Cell 18:379–391
15. Zhao BG, Smallwood A, Yang JS, Koretke K, Nurse K, Calamari A, Kirkpatrick RB, Lai ZH (2008) Modulation of kinase–inhibitor interactions by auxiliary protein binding: crystallography studies on aurora A interactions with VX-680 and with TPX2. Protein Sci 17:1791–1797
16. Heron NM, Anderson M, Blowers DP, Breed J, Eden JM, Green S, Hill GB, Johnson T, Jung FH, McMiken HHJ, Mortlock AA, Pannifer AD, Pauptit RA, Pink J, Roberts NJ, Rowsell S (2006) SAR and inhibitor complex structure determination of a novel class of potent and specific aurora kinase inhibitors. Bioorg Med Chem Lett 16:1320–1323
17. Andersen CB, WanY CJW, Riggs B, Lee C, Liu Y, Sessa F, Villa F, Kwiatkowski N, Suzuki M, Nallan L, Heald R, Musacchio A, Gray NS (2008) Discovery of selective aminothiazole aurora kinase inhibitors. ACS Chem Biol 3:180–192
18. D'Alise AM, Amabile G, Iovino M, Di Giorgio FP, BartiromoM SF, Villa F, Musacchio A, Cortese R (2008) Reversine, a novel aurora kinases inhibitor, inhibits colony formation of human acute myeloid leukemia cells. Mol Cancer Ther 7:1140–1149
19. Rawson TE, Ruth M, Blackwood E, Burdick D, Corson L, Dotson J, Drummond J, Fields C, Georges GJ, Goller B, Halladay J, Hunsaker T, Kleinheinz T, Krell HW, Li J, Liang J, Limberg A, McNutt A, Moffa J, Phillips G, Ran YQ, Safina B, Ultsch M, Walker L, Wiesmann C, Zhang BR, Zhou AH, Zhu BY, Ruger P, Cochran AG (2008) A pentacyclic aurora kinase inhihitor (AKI-001) with high in vivo potency and oral bioavailability. J Med Chem 51:4465–4475
20. Anderson K, Lai ZH, McDonald OB, Stuart JD, Nartey EN, Hardwicke MA, Newlander K, Dhanak D, Adams J, Patrick D, Copeland RA, Tummino PJ, Yang JS (2009) Biochemical characterization of GSK1070916, a potent and selective inhibitor of aurora B and aurora C kinases with an extremely long residence time. Biochem J 420:259–265
21. Morris GM, Goodsell DS, Halliday RS, Huey R, Hart WE, BelewRK OAJ (1998) Automated docking using a Lamarckian

genetic algorithm and an empirical binding free energy function. J Comput Chem 19:1639–1662
22. Wang JM, Wolf RM, Caldwell JW, Kollman PA, Case DA (2004) Development and testing of a general AMBER force field. J Comput Chem 25:1157–1174
23. Jorgensen WL (1982) Revised TIPS for simulations of liquid water and aqueous solutions. J Chem Phys 77:4156–4163
24. Ryckaert JP, Ciccotti G, Berendsen HJC (1977) Numerical integration of the Cartesian equations of motion of a system with constraints: molecular dynamics of n-alkanes. J Comput Phys 23:327–341
25. Darden T, York D, Pedersen L (1993) Particle mesh Ewald: an N-log(N) method for Ewald sums in large systems. J Chem Phys 98:10089–10092
26. Huo S, Wang J, Cieplak P, Kollman PA, Kuntz ID (2002) Molecular dynamics and free energy analyses of cathepsin D–inhibitor interactions: insight into structure-based ligand design. J Med Chem 45:1412–1419
27. Kollman PA, Massova I, Reyes C, Kuhn B, Huo S, Chong L, Lee M, Lee T, Duan Y, Wang W, Donini O, Cieplak P, Srinivasan J, Case DA, Cheatham TE (2000) Calculating structures and free energies of complex molecules: combining molecular mechanics and continuum models. Acc Chem Res 33:889–897
28. Massova I, Kollman PA (2000) Combined molecular mechanical and continuum solvent approach (MM PBSA/GBSA) to predict ligand binding. Perspect Drug Discov Des 18:113–135
29. Yan CL, Xiu ZL, Li XH, Li SM, Hao C, Teng H (2008) Comparative molecular dynamics simulations of histone deacetylase-like protein: binding modes and free energy analysis to hydroxamic acid inhibitors. Proteins 73:134–149
30. Gohlke H, Kiel C, Case DA (2003) Insights into protein–protein binding by binding free energy calculation and free energy decomposition for the Ras–Raf and Ras–RaIGDS complexes. J Mol Biol 330:891–913
31. Myrianthopoulos V, Magiatis P, FerandinY SAL, Meijer L, Mikros E (2007) An integrated computational approach to the phenomenon of potent and selective inhibition of aurora kinases B and C by a series of 7-substituted indirubins. J Med Chem 50:4027–4037
32. Howard S, Berdini V, Boulstridge JA, Carr MG, Cross DM, Curry J, Devine LA, Early TR, Fazal L, Gill AL, Heathcote M, Maman S, Matthews JE, McMenamin RL, Navarro EF, O'Brien MA, O'Reilly M, Rees DC, Reule M, Tisi D, Williams G, Vinkovic M, Wyatt PG (2009) Fragment-based discovery of the pyrazol-4-yl urea (AT9283), a multitargeted kinase inhibitor with potent Aurora kinase activity. J Med Chem 52:379–388
33. Cheetham GMT, Knegtel RMA, Coll JT, Renwick SB, Swenson L, Weber P, Lippke JA, Austen DA (2002) Crystal structure of Aurora-2, an oncogenic serine/threonine kinase. J Biol Chem 227:42419–42422
34. Lan P, Chen WN, Sun PH, Chen WM (2011) 3D-QSAR and molecular docking studies of azaindole derivatives as Aurora B kinase inhibitors. J Mol Model 17:1191–1205